RESEARCH ARTICLE

Safety and image quality at 7T MRI for deep brain stimulation systems: Ex vivo study with lead-only and full-systems

Bhumi Bhusal[1], **Jason Stockmann**[2,3], **Bastien Guerin**[2,3], **Azma Mareyam**[3], **John Kirsch**[3], **Lawrence L. Wald**[2,3], **Mark J. Nolt**[4], **Joshua Rosenow**[4], **Roberto Lopez-Rosado**[5], **Behzad Elahi**[5], **Laleh Golestanirad**[1,6]*

1 Department of Radiology, Northwestern University, Chicago, IL, United States of America, 2 Department of Radiology, Harvard Medical School, Boston, MA, United States of America, 3 Athinoula A. Martinos Center for Biomedical Imaging, Massachusetts General Hospital, Boston, MA, United States of America, 4 Department of Neurosurgery, Northwestern University, Chicago, IL, United States of America, 5 Department of Physical Therapy and Human Movement Sciences, Northwestern University, Chicago, IL, United States of America, 6 Department of Biomedical Engineering, Northwestern University, Evanston, IL, United States of America

* Laleh.rad1@northwestern.edu

Abstract

Ultra-high field MRI at 7 T can produce much better visualization of sub-cortical structures compared to lower field, which can greatly help target verification as well as overall treatment monitoring for patients with deep brain stimulation (DBS) implants. However, use of 7 T MRI for such patients is currently contra-indicated by guidelines from the device manufacturers due to the safety issues. The aim of this study was to provide an assessment of safety and image quality of ultra-high field magnetic resonance imaging at 7 T in patients with deep brain stimulation implants. We performed experiments with both lead-only and complete DBS systems implanted in anthropomorphic phantoms. RF heating was measured for 43 unique patient-derived device configurations. Magnetic force measurements were performed according to ASTM F2052 test method, and device integrity was assessed before and after experiments. Finally, we assessed electrode artifact in a cadaveric brain implanted with an isolated DBS lead. RF heating remained below 2°C, similar to a fever, with the 95% confidence interval between 0.38°C-0.52°C. Magnetic forces were well below forces imposed by gravity, and thus not a source of concern. No device malfunctioning was observed due to interference from MRI fields. Electrode artifact was most noticeable on MPRAGE and T2*GRE sequences, while it was minimized on T2-TSE images. Our work provides the safety assessment of ultra-high field MRI at 7 T in patients with DBS implants. Our results suggest that 7 T MRI may be performed safely in patients with DBS implants for specific implant models and MRI hardware.

Introduction

Deep brain stimulation (DBS) therapy is among the most important advances in clinical neuroscience over the past two decades. DBS involves an initial neurosurgical procedure to implant electrodes into specific targets within the brain, that then deliver constant or intermittent electrical pulses via an implanted pulse generator (IPG) to modulate aberrant neural behavior. DBS is currently the gold standard treatment for drug-resistant Parkinson's disease and essential tremor and has received humanitarian device exemption for treatment of dystonia and obsessive-compulsive disorder. In addition, there are numerous clinical trials currently underway or recently completed to evaluate the efficacy of DBS in treating other disorders, most notably chronic pain, epilepsy, major depression, and Alzheimer's disease.

It is estimated that 70% of patients with DBS implants will need magnetic resonance imaging (MRI) within 10 years of their implantation [1]. Despite tremendous potential of MRI and fMRI to guide DBS therapy, safety concerns have limited post-operative accessibility of MRI to patients with DBS devices, mainly due to fatal injuries resulting from radiofrequency (RF) heating of DBS leads during the transmit phase of MRI [2]. For this reason, strict conditions have been put in place to perform MRI in DBS patients, namely, majority of DBS systems are approved for horizontal 1.5 T scanners using pulse sequences with $B_1^+RMS<2\mu T$ [3–5].

To date, studies that have assessed the safety and feasibility of postoperative MRI for DBS imaging have focused on 1.5 T and 3 T scanners due to their clinical prevalence [2, 6–10]. Ultra-high field MRI at 7 T provides promise to push the boundaries of DBS target visualization [11], yet no study has assessed safety and image quality of 7 T MRI in patients with DBS devices. Here we report results of RF heating assessment, magnetic force measurement, and image artifact of a commercial DBS device implanted in an anthropomorphic phantom undergoing MRI at 7 T. RF heating measurements were performed with 43 unique device configurations based on realistic lead trajectories extracted from postoperative CT images of patients. A multi-material anthropomorphic phantom was constructed and used to maximize the resemblance of RF exposure experiments to what happens *in vivo*. Magnetic force measurements were performed according to ASTM F2052-15 [12]. Finally, we assessed the metal artifact around implanted leads in a cadaveric brain using imaging sequences optimized for DBS target visualization.

Our results provide relevant data to assess RF safety of MRI in patients with DBS devices.

Materials and methods

Magnetic resonance imaging equipment and imaging protocols

Experiments were performed on a 7 T scanner (MAGNETOM; Siemens Healthineers, Erlangen, Germany) using a home-made local transmit/receive head coil. The coil used in experiments was an 8-channel wrap-around receive array, nested inside a shielded detunable quadrature birdcage volume coil (Fig 1). The volume coil slid (in the bore direction) to increase accessibility for the patient/phantom. The receive array helmet was sized to accommodate a majority of adult heads and was large enough to fit the phantom. It comprised of 8 overlapped rectangular elements (6.5 cm x 13 cm), built on 8 panels that were arranged in a u-shape around the head. A 3D-printed hinge mechanism used between neighboring panels allowed the array to be wrapped closely around phantom's head to provide a high filling factor and maximal SNR. Flexible copper braid was used over the panel joints to allow the hinges to move without breaking each coil's conducting path. Each loop was made of 16 AWG wire with seven or eight evenly-spaced tuning capacitors. All elements were tuned to 297.2 MHz and matched when loaded to an impedance of 75 Ω to minimize the noise figure of the Siemens 7T preamplifiers.
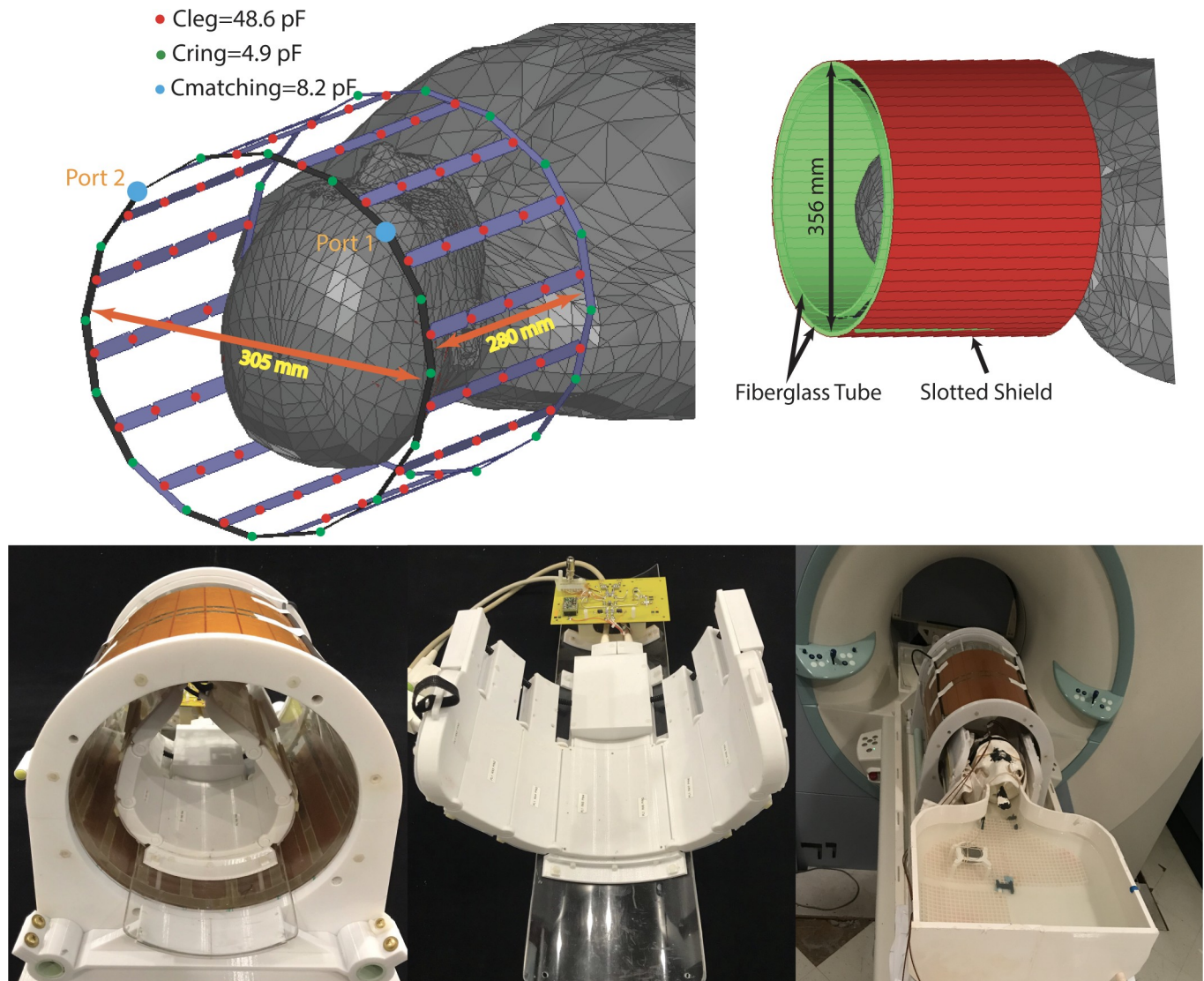
Fig 1. RF coil and phantom configurations.

The transmit coil was a detunable 16-rung band-pass birdcage with a rung length of 28 cm and diameter of 30.5 cm which was nested inside a cylindrical slotted shield. Birdcage conductors were routed out of 7.8 mm circuit board and then bent and fastened to the inner surface of a fiberglass tube. The birdcage coil was tuned to 297.2 MHz using 16x4.9 pF capacitors distributed around each end ring and 5x48.6 pF capacitors distributed along each leg. Series capacitors of 8.2 pF were used to match the coil a loaded impedance of 50 Ω. Drive ports were located at the top front side of the coil (see Fig 1).

RF heating measurements were performed during 7 minutes of imaging with a T_2W HASTE sequence (32 averages), where TE, TR and echo spacing parameters were adjusted to reach the maximum SAR allowed by the scanner. For B_1^+ estimation, we aquired flip angle maps in the phantom using Siemens's tfl_WIP543_B1map pulse sequence with TE = 2.14 ms, TR = 2000 ms and nominal flip angle of 90˚. The flip angle maps were then converted to maps of B_1^+/Volt which was the B_1^+ produced by the coil per unite of voltage exication. These maps

Table 1. Sequence parameters for HASTE sequence used for RF heating measurements.

T2W-HASTE	
TE (msec)	99
TR (msec)	2000
FOV (mm)	200
FA	180
Echo Spacing (msec)	4.96
Turbo Factor	319
TA	7:04
No of Slices	6
Slice thickness (mm)	2
Resolution (mm)	0.6x0.6x2.0
Averages	32
B_1^+RMS (μT)	2.88
Most Critical Safety Aspect	Local Head SAR 10 W/kg

TE = Echo time, TR = Repetition time, FOV = Field of view, FA = Flip Angle, TA = Acquisition time.

https://doi.org/10.1371/journal.pone.0257077.t001

were then used to estimate the B_1^+RMS during the HASTE sequence. HASTE sequence parameters for RF heating measurements are summarized in Table 1.

Electrode artifact was assessed on MPRAGE, T_2W TSE and T_2^*W GRE images with parameters that were reported to optimize visualization of subthalamic nucleus in patients [13, 14]. Details of sequence parameters for image artifact assessment are reported in Table 2.

Anthropomorphic phantom and DBS device configurations

It is well established that RF heating of elongated conductive implants (such as leads) is highly dependent on the trajectory of the implant and distribution of MRI electric fields in the sample and around the implant [15–22]. To have a more realistic field distribution around the implanted lead, we used a multi-material anthropomorphic phantom consisting of a 3D-printed body-shaped container and a refillable skull structure, with the design based on CT images of a patient with a DBS device. Use of patient data for the purpose of MRI RF heating assessment and publication of de-identified images was approved by Northwestern University's Institutional Review Board (STU00206859). Consent was waived as the data was collected retrospectively and analyzed anonymously.

Table 2. Sequence parameters for image artifact study.

Parameters	Sequence		
	MPRAGE	T_2W- TSE	T_2^*W-GRE
TE (msec)	1.74, 3.68	58	17.8
TR (msec)	2530	8000	501
FOV (mm)	165	163	176
FA	7	131	40
TA	8:53	9:28	6.27
No of Slices	224	80	17
Slice thickness (mm)	0.8	1	1
Resolution (mm)	0.8x0.8x0.8	0.4x0.4x1.0	0.5x0.5x1.0
Averages	2	2	2

TE = Echo time, TR = Repetition time, FOV = Field of view, FA = Flip Angle, TA = Acquisition time.

https://doi.org/10.1371/journal.pone.0257077.t002

Details of phantom design and construction are described elsewhere [23]. In brief, the skull was filled with a tissue mimicking gel, prepared by mixing 32 g/L of edible agar (Landor Trading Company, gel strength 900 g/cm2) with saline solution (2.25 gNaCL/L) with electric conductivity of $\sigma = 0.43$ S/m, similar to values reported for brain tissue [24]. Once cooled down to room temperature, the mixture formed a semi-solid gel which kept the DBS lead in place, and had the thermal conductivity of ~0.56 J/K-S [25] similar to that of grey matter [26].

DBS surgery is usually performed at two stages: first, electrodes are implanted in the target nuclei with the extracranial portion of the lead routed under the scalp, and the patient is sent home to recover. In a second surgery leads are connected to extensions, which are then routed subcutaneously down the neck toward the pectoral region and connected to the IPG. MRI in patients with lead-only systems is useful for target verification, but a majority of MRI exams, including those that study functional effect of stimulation, are performed in patients with fully implanted DBS systems. We replicated 28 configurations for lead-only systems (11 configurations with Medtronic lead 3387, and 17 configurations with Medtronic lead 3389) and 15 configurations for a fully implanted DBS system (Medtronic lead 3389, extension 3708660, IPG Activa SC-37603) for RF heating experiments. Fig 2 shows typical DBS lead trajectories from post-operative CT images of patients as well as some that were replicated in the phantom.
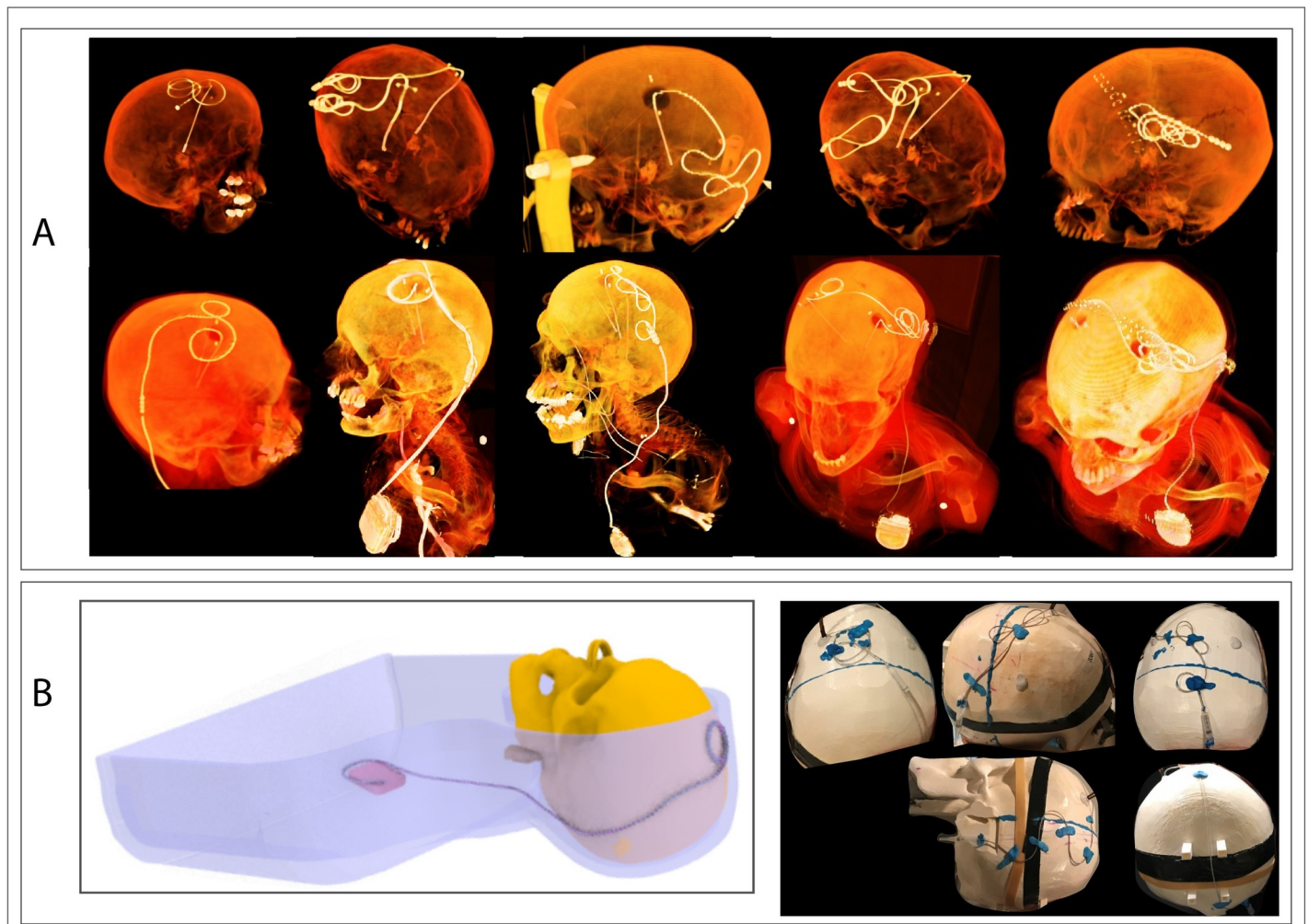
Fig 2. DBS trajectory configurations. (A) 3D-rendered postoperative CT images of DBS patients showing typical trajectories of extra-cranial leads and extensions. (B) Schematic of the phantom implanted with a full DBS device as well as examples of some trajectories used in RF heating experiments.
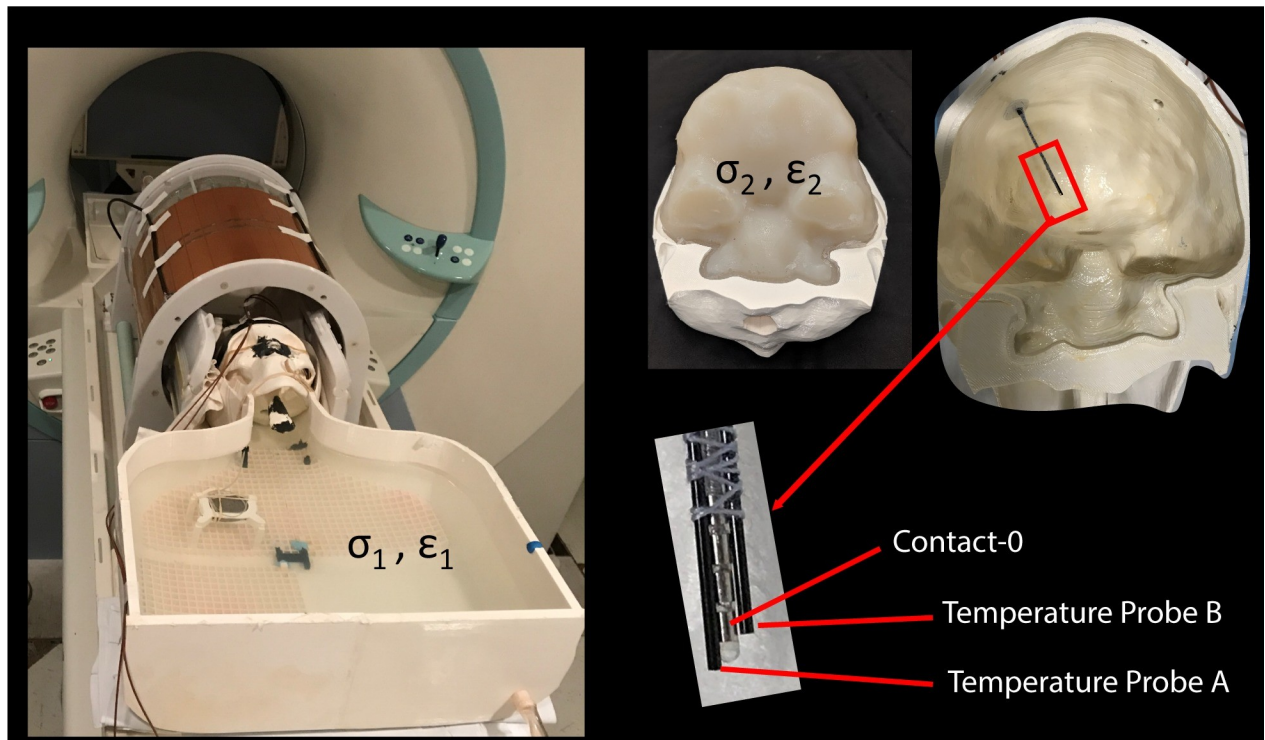
Fig 3. Experimental setup for RF heating measurements. Experimental setup with saline-filled anthropomorphic phantom (ε_1 = 78, σ_1 = 0.51 S/m) and gel-filled skull (ε_2 = 75, σ_2 = 0.43 S/m). Positioning of temperature probes at the tip of lead model 3389 is also shown.

https://doi.org/10.1371/journal.pone.0257077.g003

RF heating measurements

Two MR-compatible fluoptic temperature probes (OSENSA, BC, Canada, resolution 0.01˚C) were secured close to electrode contact 0 of Medtronic DBS leads (Medtronic model 3387 or 3389) as shown in Fig 3. One probe was positioned such that it was in touch with the electrode contact itself, and the other was secured one millimeter further distally such that its tip was in contact with the gel. This allowed us to assess the spatial profile of RF heating around the DBS lead's tip. The ensemble of lead-probe system was inserted into the gel-filled skull through a 5 mm hole following entry point, angle, and penetration depth analogous to the clinical approach for targeting the left subthalamic nucleus. The skull structure containing the lead-probe system was inserted into the phantom's body container which was then filled with the saline solution (conductivity of σ = 0.51 S/m representing average tissue). In cases with a complete DBS system, the lead was connected to an extension (Medtronic model 3708660) and an implanted pulse generator (IPG) (Medtronic Activa SC-37603), with the IPG positioned either at the right pectoral region to create contralateral configuration or at the left pectoral region to create an ipsilateral configuration. The former (contralateral configuration) is shown to generally generate higher RF heating [27].

Magnetic force measurements

Magnetically induced displacement force on the pulse generator produced by the spatial gradient of the static magnetic field was measured according to ASTM F2052 test method [12]. A home-made test fixture was designed and fabricated consisting of a nonmagnetic 3D-printed sturdy structure capable of holding the IPG in proper position without deflection (see Fig 4).
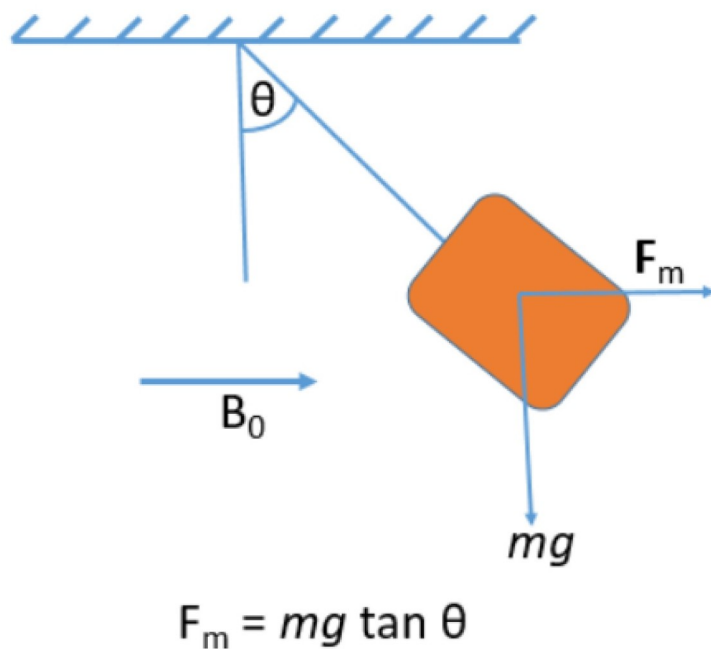
Fig 4. Force measurement setup.

The IPGs (Medtronic Activa PC-37601 and Activa SC-37603) were suspended (one at a time) by a string and the angular deflection of the string from the vertical was measured at a location near the entrance of the scanner bore where the spatial gradient of $\Delta\boldsymbol{B_0} = dB_0/dz$ was maximum as well as several other locations along the bore. If the device deflects less than 45˚, then the magnetically induced deflection force is less than the force on the device due to gravity (its weight). For this condition, it can be assumed that any risk imposed by the application of the magnetically induced force is no greater than any risk imposed by normal daily activity in the Earth's gravitational field.

Image artifact

To assess the image artifact, the gel-filled skull was replaced with a similar 3D-printed skull structure which contained a formalin-fixed cadaveric brain which was donated to Northwestern Medical School for educational and research purposes. None of the transplant donors were from a vulnerable population and all donors or next of kin provided written informed consent that was freely given. An isolated Medtronic DBS lead (model 3387) was implanted into the subthalamic nucleus of the cadaver brain as described in previous work [28]. Steps of preparing and implanting the DBS into the cadaver brain are given in Fig 5. The brain-containing skull was then placed inside the saline-filled torso of the phantom and scanned using MPRAGE, T_2W-TSE, and $T_2{}^*$W-GRE sequences with details given in Table 2. Images were imported into 3D slicer (Slicer 4.10, www.slicer.org) and the width of the artifact around the DBS contacts was measured manually.
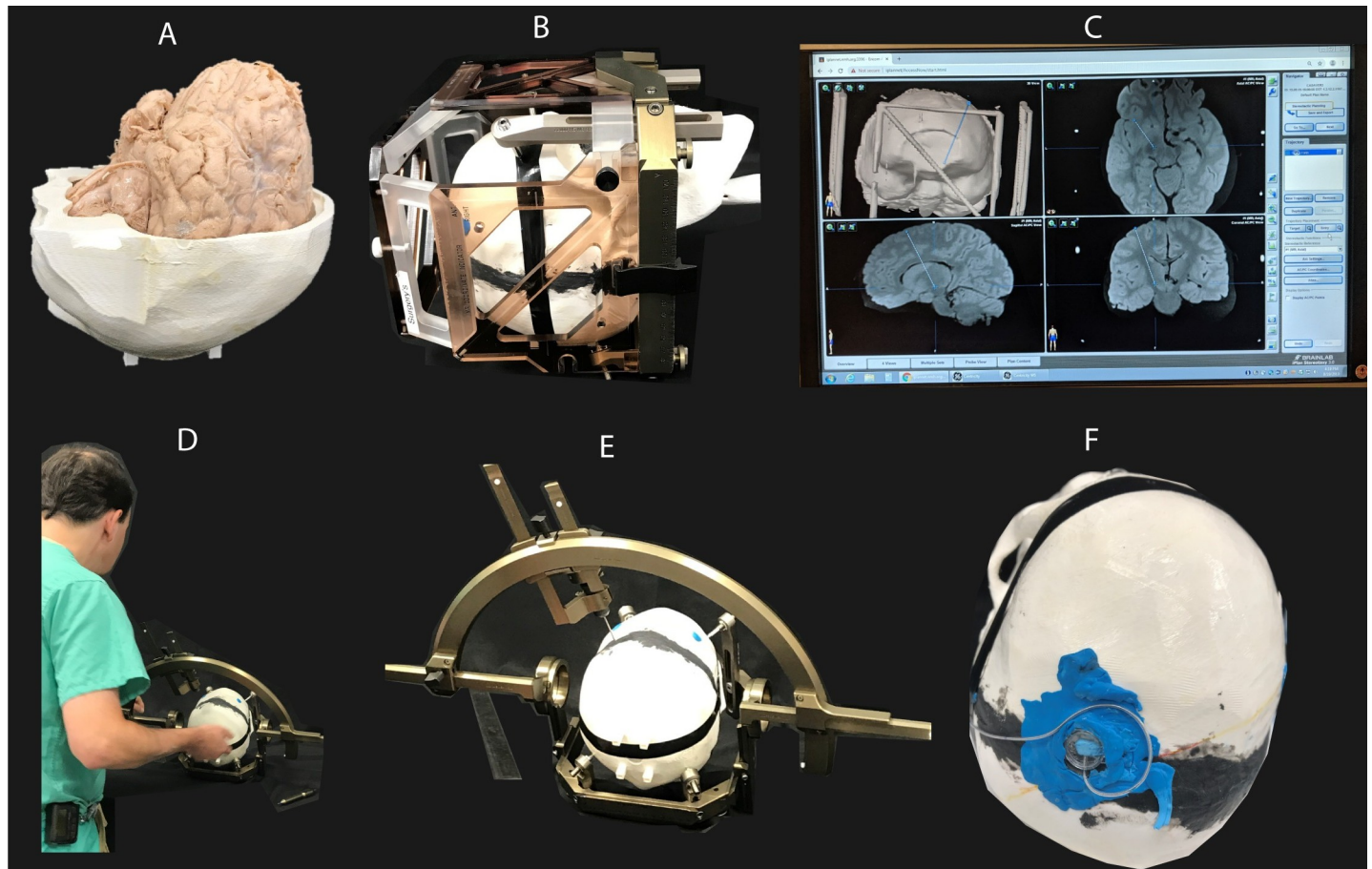
Fig 5. Steps of implanting DBS lead into a cadaver brain. (A) A formalin-fixed cadaveric brain was contained inside a 3D printed skull structure which was then filled with formalin solution. (B) The skull was attached to a Lakesell model G base ring (Elekta, Stockholm, Sweden) using titanium fixation pins, placed inside MRI fiducial box, and scanned at 1.5T for localizing subthalamic nucleus. (C) Images from MRI scan were transferred to BrainLAB iPlan server for determining coordinates of subthalamic nucleus as well as the entry point of the DBS lead on the skull. (D-F) A StimLoc ring was attached to the skull for the electrode implantation. After implanting the DBS lead, the StimLock ring was removed and a burr hole cover was placed to fixate the lead at the entry point.

https://doi.org/10.1371/journal.pone.0257077.g005

Assessment of DBS system integrity

Before starting the experiments, we verified the integrity of the implanted DBS system by measuring the inter-electrode as well as electrode-IPG impedances (for fully implanted systems) as recommended by the manufacturer. The IPG was set to "stimulation off" during experiments. Impedance measurements were also repeated after MRI experiments to ensure RF exposure did not impair the device function.

Results

RF heating

Table 3 gives the temperature rise at tips of leads 3389 and 3387 configured along different trajectories, measured by probe A at the end of a 7-minute scan with the T_2W HASTE sequence. The maximum difference in recorded temperatures by probes A and B was less than 0.06°C. The mean±std temperature rise ΔT was 0.58±0.23°C for the lead-only system with lead 3387, 0.57±0.30°C for the lead-only system with lead 3389, and 0.52±0.32°C for the full system (lead

Table 3. Temperature rise for lead-only and full DBS configurations.

Lead only-3389		Lead only-3387		Full system	
config. #	ΔT [˚C]	config. #	ΔT [˚C]	config. #	ΔT [˚C]
1	1.06	1	0.68	1	1.01
2	0.54	2	1.08	2	0.22
3	0.8	3	0.6	3	0.37
4	0.42	4	0.59	4	0.77
5	0.22	5	0.46	5	0.49
6	0.52	6	0.34	6	1.07
7	0.35	7	0.89	7	0.63
8	0.71	8	0.34	8	0.45
9	0.51	9	0.58	9	0.24
10	0.46	10	0.38	10	0.22
11	1.36	11	0.47	11	0.31
12	0.27	-	-	12	0.19
13	0.3	-	-	13	0.17
14	0.84	-	-	14	0.86
15	0.45	-	-	15	0.84
16	0.56	-	-	-	-
17	0.35	-	-	-	-

3389+extension 3708660+IPG Activa PC-37601). A single factor ANOVA showed no significant difference in the ΔT between groups (P-value = 0.84).

Fig 6A shows distribution of the pooled data (ΔT from all three groups, n = 43) fitted to a Rayleigh probability distribution (σ = 0.44, standard error = 0.03) using MATLAB R2019a *Distribution Fitter* app. Under this distribution, the 95% confidence interval of ΔT is estimated to fall between 0.38˚C-0.52˚C. Fig 6B shows lead configurations that generated the maximum (ΔT = 1.4˚C), minimum (ΔT = 0.2˚C), and average (ΔT = 0.5˚C) temperature rise for the fully implanted DBS system, along with their temporal heating profile.

Induced magnetic force and system integrity

The maximum deflection angle was observed when the IPG was hung close to the scanner wall at the entrance of the bore and was measured to be 25˚ for the IPG model Activa PC (Model 37601) and 36˚ for the model Activa SC (Model 37603). This means that the magnetic forces experienced during the scan do not pose a risk greater than the exposure of the device to Earth's gravitational forces. Measured impedance values before and after RF heating experiments were within the manufacturer's recommended range, namely <4000 Ω for inter-electrode impedances and <2000 Ω for electrode-IPG impedances and also with no short circuits.

Image artifact

The image artifacts around the DBS lead produced during MRI imaging with different routine clinical sequences (Table 2) are shown in the Fig 7. The artifact diameter around the electrode contacts of the DBS lead were measured on transverse as well as coronal planes as depicted in the Fig 7. The average size of the artifact (averaged between transverse and coronal slice for each sequence) around the DBS contacts was observed to be 4.7 mm, 5.4 mm and 7.3 mm for the sequences T2-TSE, MPRAGE and T2*-GRE respectively.
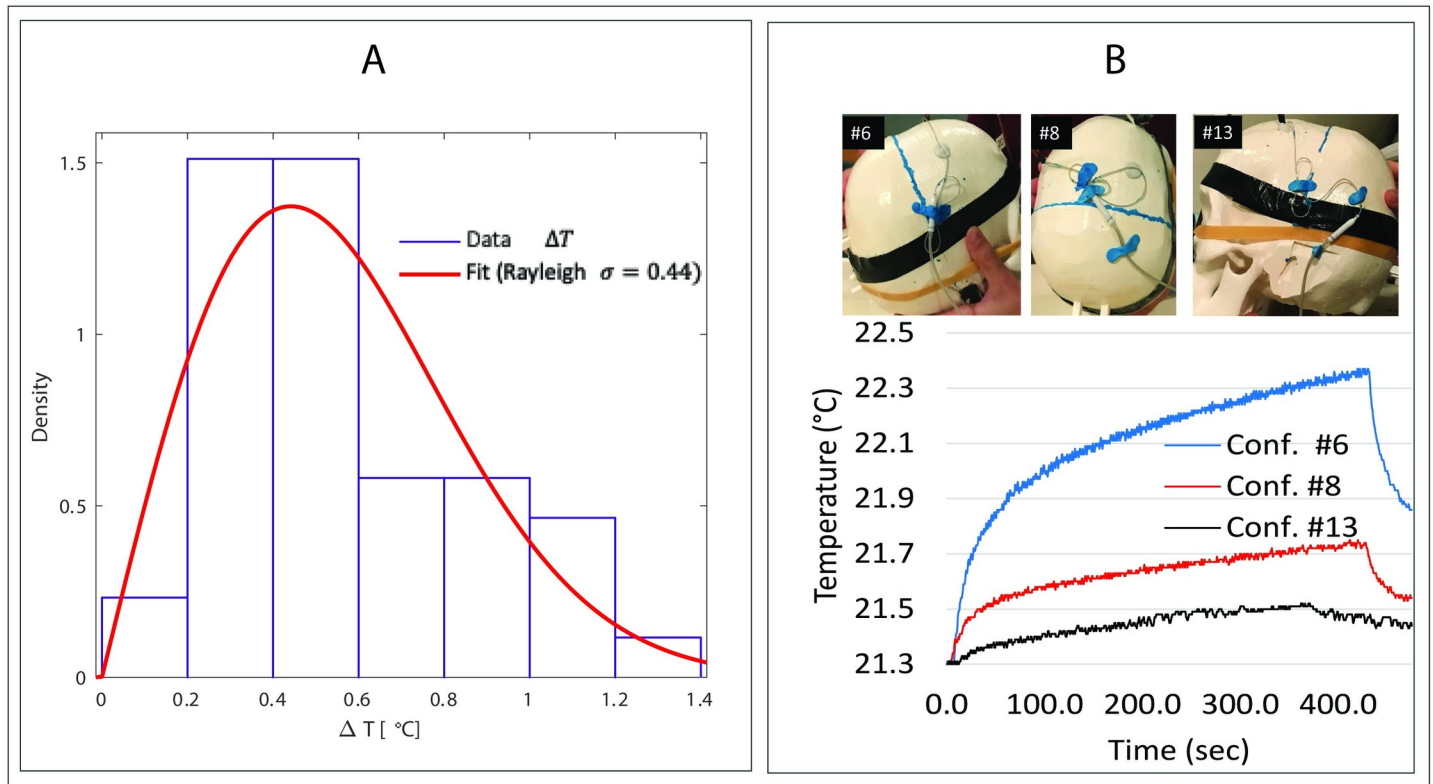
Fig 6. RF heating results. (A) Distribution of pooled data (n = 43) fitted to a Rayleigh probability distribution MATLAB. (B) Temporal profile of temperature rise for three configurations (Conf #6, #8 and #13 as shown in the attached pictures) for full DBS system, representing maximum, intermediate and the minimum heating scenarios.

Discussion

The rising prevalence of chronic diseases coupled with the rapidly aging population worldwide has made medical implants more ubiquitous than ever [29, 30]. More than 12 million Americans currently carry a form of orthopedic, cardiovascular, or neuro-modulation device and the number grows by 80,000 annually. It is estimated that 50%-75% of patients with conductive implants will need to undergo MRI during their lifetime [31], with many patients requiring repeated examinations [32].

Advances in device engineering have led to a new generation of electronic implants that are largely immune to MRI-generated static and gradient fields. Tissue heating from radiofrequency (RF) excitation fields, however, remains a major issue. This *"antenna effect"* [33–35] happens when the electric field of the MRI transmitter couples with implanted leads, causing the specific absorption rate (SAR) of the RF energy to significantly amplify at the implant's tip [36]. Given the potential for fatal hazards, the conditions under which patients with conductive implants are indicated for MRI are restrictive. In patients with DBS devices for example, MRI is allowed only at 1.5T field strength for majority of devices, using pulse sequences with a SAR of 0.1 W/kg (30 times below FDA limit for scanning in absence of implants) or $B_1^+RMS<2\mu T$, and the current state-of-the-art neuroimaging techniques at 3T and above are contraindicated [3–5]. There is strong incentive, however, toward use of high and ultra-high field MRI to inform DBS therapy:1.) 1.5T MRI systematically underestimates the anterior and lateral boundaries of the subthalamic nucleus (STN) and globus pallidus (common DBS targets) compared to fast gray matter T1 inversion recovery acquisitions at higher fields [37], and
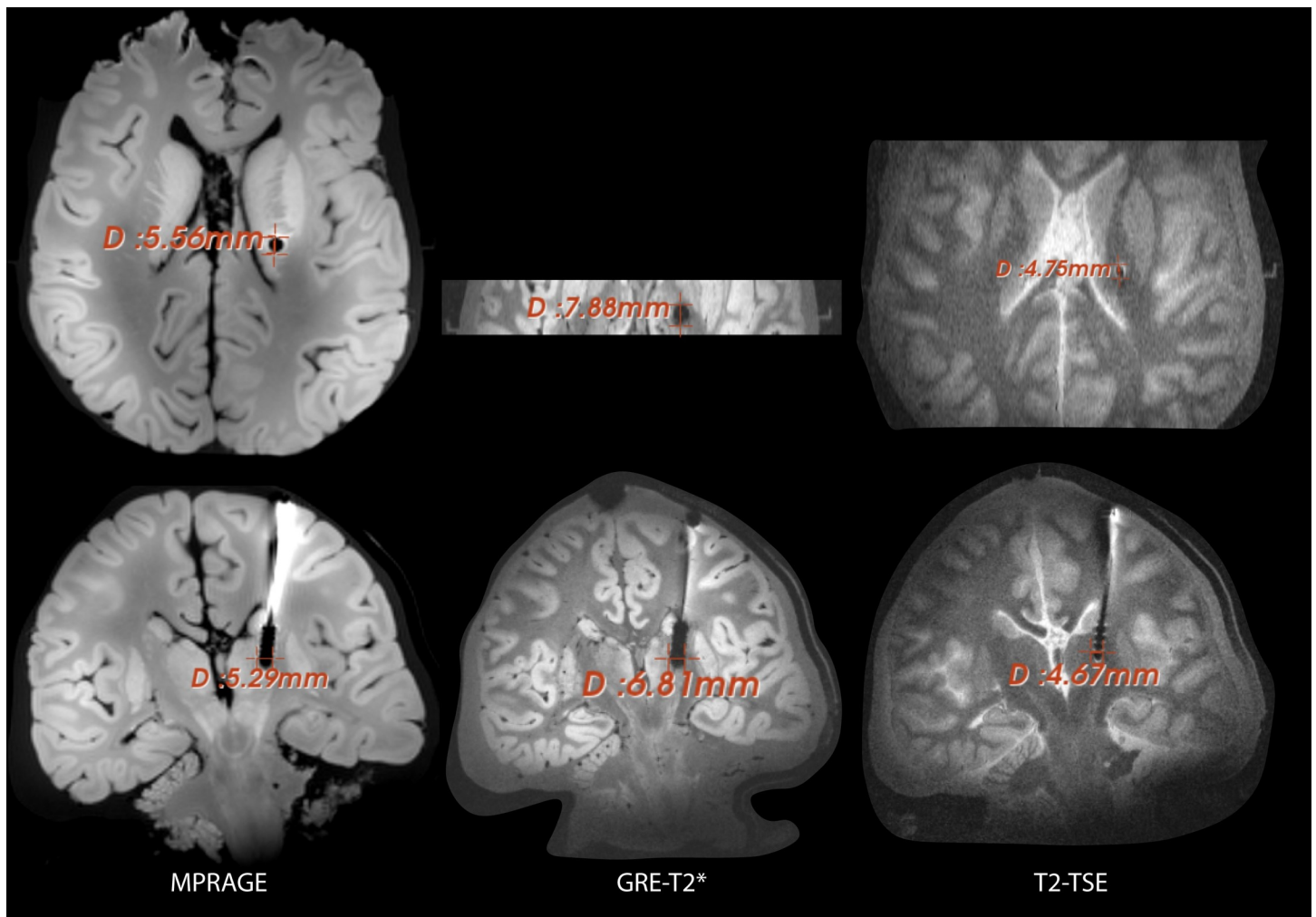
Fig 7. Image artifact measurements. Image artifact around the DBS lead implanted into the cadaveric brain. Each column represents the artifact in transverse and coronal planes for sequences detailed in Table 2. The artifact size (width) around electrode contacts is reported for each case. Scans were performed with a lead-only system, with the extra-cranial portion of the lead looped around the bur hole.

https://doi.org/10.1371/journal.pone.0257077.g007

2.) high-field MRI confers a much better contrast-to-noise ratio which makes it easier to delineate small abutting structures [38]. Given that DBS targets such as the STN, are bordered by several small structures (e.g, the ansa lenticularis, zona incerta, and substanitia nigra), this capacity becomes crucial. Finally, high-field MRI is more sensitive to susceptibility artifacts which acts as an advantage when visualizing the iron-rich STN [39, 40] and helps delineate pallidofugal and striatonigral fiber tracts, further aiding electrode positioning [41].

The past few years have witnessed a spike in engineering efforts to realize *implant-friendly* MRI for patients with DBS implants. Pioneering work has been done to advance MRI field-shaping methods,—techniques that manipulate the electric field of MRI transmit coil to eliminate its interaction with individual patient's implants [6, 8, 42–49]. Another alternative approach is surgical device management, where trajectories of implanted leads are surgically modified (based on computer simulations) such that their coupling with MRI electric fields is minimized [21, 50]. Finally, there has been a spate of patents and papers proposing novel implant structures [51–55] and materials [56, 57] to reduce induced RF currents, and by proxy, RF heating. Despite the promising potential of these innovations to make state-of-the-

art MRI accessible to patients with DBS implants, their clinical translation has been very slow. As a result, researchers have resorted to application of MRI beyond the currently approved labeling of the device based on RF heating assessment through phantom experiments or numerical simulations. These studies, however, have focused on 1.2T, 1.5T and 3T scanners due to their clinical prevalence [10, 58–62]. This work presents the first study of MRI safety in patients with DBS implants at 7T, and as such, provides a frame of reference to compare risks and benefits of ultra-high field MRI in this patient population.

The technical specification ISO-TS 10974 provides insights into different mechanisms that could potentially cause hazard during MRI in patients with active electronic implants [63]. Specifically, most prominent sources of hazard known today are electrode heating, unintended stimulation, device heating, device malfunction and device vibration, as well as dislodgment due to magnetic force and torque. In terms of electrode heating, our results show that at 7T, the maximum heating for a wide range of clinically relevant as well as worst-case scenarios remains well below 2˚C, similar to a fever.

Other sources of hazard include device vibration and/or malfunction, device dislodgement due to magnetic forces, and unintended stimulation. Unintended tissue stimulation is a source of concern where leads are in touch with cardiac tissue, such as in cardiovascular implanted electronic devices, as stimulation could cause arrythmia. In DBS patients, such effect has not been observed [58] and may not be a potential concern. Device vibration could happen due to MRI gradient fields and is only relevant for implants with large conductive plates and not a source hazard for implanted leads [63]. Also, in our experiments, we did not notice any vibration in the IPG during the scans. With regard to magnetic force, our measurements showed that such forces were well below the limit that could potentially pose any risk. Finally, for the specific device model that was tested, system integrity verification ruled out the possibility of device malfunction due to damages caused by MRI fields. We would like to note, however, that results of this study should not be interpreted as proof for safety of scanning patients with DBS devices at 7T in a similar way that MR-conditional labeling of such devices do. Specifically, more tests are required to assure all aspects of patient and device safety are evaluated as laid out in ISO-TS 10974. This result of this work should be only interpreted as a preliminary assessment that would incentivize performing more thorough tests that lead to labeling of DBS devices at 7T.

In terms of image quality, 7T MRI is shown to allow direct and clear visualization of the small and deep cortical structures such as the STN—a main target in DBS for treating Parkinson's disease [11, 13]. However, as the high field MRI is prone to increased susceptibility artifacts, the image artifacts around the DBS contacts could be a drawback of using 7T MRI for target verification. For the particular model of DBS lead used in this study, we observed that the artifact size (4-6mm) was comparable to the size of the STN [64]. Which means, for a properly positioned DBS lead, the STN or similar sized targets might be fully or mostly masked by the artifact. However, due to clear direct visualization of the neighboring structures, such as substantia nigra at 7 T, it may be still possible to verify the position of the DBS lead relative to the target nucleus. Specifically, Fig 7 shows a substantially smaller artifact for a spin echo sequence (T2-TSE in Table 2) compared to gradient echo or MPRAGE as recommended in the earlier study [65]. Also, as the size of the artifact may depend upon the lead geometry, the results may differ among lead models.

Conclusion

This work provides the first safety assessment of ultra-high field MRI at 7T in patients with DBS implants. Our results suggest that 7T MRI may be performed safely in patients with DBS

implants for specific implant models and MRI hardware. However, these results should not be generalized to other models of DBS implants that have not been tested here, or to other 7T MRI hardware.

Author Contributions

Conceptualization: Bhumi Bhusal, Laleh Golestanirad.

Data curation: Bhumi Bhusal, Bastien Guerin, Laleh Golestanirad.

Formal analysis: Bhumi Bhusal, Behzad Elahi, Laleh Golestanirad.

Funding acquisition: Laleh Golestanirad.

Investigation: Bhumi Bhusal, Jason Stockmann, Azma Mareyam, John Kirsch, Mark J. Nolt, Joshua Rosenow, Laleh Golestanirad.

Methodology: Bhumi Bhusal, Jason Stockmann, Bastien Guerin, John Kirsch, Laleh Golestanirad.

Project administration: Bhumi Bhusal, Laleh Golestanirad.

Resources: Jason Stockmann, Lawrence L. Wald, Mark J. Nolt, Joshua Rosenow, Roberto Lopez-Rosado.

Supervision: Laleh Golestanirad.

Writing – original draft: Bhumi Bhusal, Laleh Golestanirad.

Writing – review & editing: Bhumi Bhusal, Behzad Elahi, Laleh Golestanirad.

References

1. Falowski S, Safriel Y, Ryan MP, Hargens L. The rate of magnetic resonance imaging in patients with deep brain stimulation. Stereotactic and functional neurosurgery. 2016; 94(3):147–53. https://doi.org/10.1159/000444760 PMID: 27245875

2. Rezai AR, Phillips M, Baker KB, Sharan AD, Nyenhuis J, Tkach J, et al. Neurostimulation system used for deep brain stimulation (DBS): MR safety issues and implications of failing to follow safety recommendations. Investigative radiology. 2004; 39(5):300–3. https://doi.org/10.1097/01.rli.0000124940.02340.ab PMID: 15087724

3. MRI Procedure Information for Abbott Medical MR Conditional Deep Brain Stimulation Systems. Clinician's Manual. Last Accessed in May 2021: https://manuals.sjm.com/Search-Form?re=North-America&cc=US&ln=all&ct=professional&qry=DBS&ipp=10.

4. ImageReady MRI Guideliens for Boston Scientific Deep Brain Stimulation Systems. Last Accessed on May 2021: https://www.bostonscientific.com/content/dam/Manuals/us/current-rev-en/92195369-01_ImageReady%E2%84%A2_MRI_Guidelines_for_Boston_Scientific_Deep_Brain_Stimulation_Systems_en-US_s.pdf.

5. Medtronic MRI guidelines for Medtronic deep brain stimulation systems. Last Accessed on May 2021: http://manuals.medtronic.com/content/dam/emanuals/neuro/M006536C_a_001_view.pdf.

6. Golestanirad L, Keil B, Angelone LM, Bonmassar G, Mareyam A, Wald LL. Feasibility of using linearly polarized rotating birdcage transmitters and close-fitting receive arrays in MRI to reduce SAR in the vicinity of deep brain simulation implants. Magnetic resonance in medicine. 2017; 77(4):1701–12. https://doi.org/10.1002/mrm.26220 PMID: 27059266

7. Golestanirad L, Kazemivalipour E, Keil B, Downs S, Kirsch J, Elahi B, et al. Reconfigurable MRI coil technology can substantially reduce RF heating of deep brain stimulation implants: First in-vitro study of RF heating reduction in bilateral DBS leads at 1.5 T. PloS one. 2019; 14(8). https://doi.org/10.1371/journal.pone.0220043 PMID: 31390346

8. Golestanirad L, Iacono MI, Keil B, Angelone LM, Bonmassar G, Fox MD, et al. Construction and modeling of a reconfigurable MRI coil for lowering SAR in patients with deep brain stimulation implants. Neuroimage. 2017; 147:577–88. https://doi.org/10.1016/j.neuroimage.2016.12.056 PMID: 28011252

9. Baker KB, Tkach J, Hall JD, Nyenhuis JA, Shellock FG, Rezai AR. Reduction of magnetic resonance imaging-related heating in deep brain stimulation leads using a lead management device. Neurosurgery. 2005; 57(4):392–7. https://doi.org/10.1227/01.neu.0000176877.26994.0c PMID: 16234691

10. Boutet A, Hancu I, Saha U, Crawley A, Xu DS, Ranjan M, et al. 3-Tesla MRI of deep brain stimulation patients: safety assessment of coils and pulse sequences. Journal of Neurosurgery. 2019; 132(2):586–94. https://doi.org/10.3171/2018.11.JNS181338 PMID: 30797197

11. Maruyama S, Fukunaga M, Fautz H-P, Heidemann R, Sadato N. Comparison of 3T and 7T MRI for the visualization of globus pallidus sub-segments. Scientific Reports. 2019; 9(1):1–8. https://doi.org/10.1038/s41598-018-37186-2 PMID: 30626917

12. ASTM F2052-15, Standard Test Method for Measurement of Magnetically Induced Displacement Force on Medical Devices in the Magnetic Resonance Environment. ASTM International, West Conshohocken, PA 2015.

13. Cho Z-H, Min H-K, Oh S-H, Han J-Y, Park C-W, Chi J-G, et al. Direct visualization of deep brain stimulation targets in Parkinson disease with the use of 7-tesla magnetic resonance imaging. Journal of neurosurgery. 2010; 113(3):639–47. https://doi.org/10.3171/2010.3.JNS091385 PMID: 20380532

14. Plantinga BR, Temel Y, Duchin Y, Uludağ K, Patriat R, Roebroeck A, et al. Individualized parcellation of the subthalamic nucleus in patients with Parkinson's disease with 7T MRI. Neuroimage. 2018; 168:403–11. https://doi.org/10.1016/j.neuroimage.2016.09.023 PMID: 27688203

15. Nordbeck P, Fidler F, Weiss I, Warmuth M, Friedrich MT, Ehses P, et al. Spatial distribution of RF-induced E-fields and implant heating in MRI. Magnetic resonance in medicine. 2008; 60(2):312–9. https://doi.org/10.1002/mrm.21475 PMID: 18666101

16. Martinez JA, Serano P, Ennis DB. Patient orientation affects lead-tip heating of cardiac active implantable medical devices during MRI. Radiology: Cardiothoracic Imaging. 2019; 1(3):e190006. https://doi.org/10.1148/ryct.2019190006 PMID: 32076667

17. Vu J, Bhusal B, Nguyen BT, Golestanirad L, editors. Evaluating Accuracy of Numerical Simulations in Predicting Heating of Wire Implants During MRI at 1.5 T. 2020 42nd Annual International Conference of the IEEE Engineering in Medicine & Biology Society (EMBC); 2020: IEEE.

18. Nguyen BT, Pilitsis J, Golestanirad L. The effect of simulation strategies on prediction of power deposition in the tissue around electronic implants during magnetic resonance imaging. Physics in Medicine & Biology. 2020. https://doi.org/10.1088/1361-6560/abac9f PMID: 32756027

19. Nguyen BT, Bhusal B, Golestanirad L. Interdependency of SAR amplification on external trajectory and internal geometry of implanted leads during MRI at 3T. Proc Intl Soc Mag Reson Med 28. 2020:4176.

20. Mattei E, Triventi M, Calcagnini G, Censi F, Kainz W, Mendoza G, et al. Complexity of MRI induced heating on metallic leads: experimental measurements of 374 configurations. Biomedical engineering online. 2008; 7(1):11. https://doi.org/10.1186/1475-925X-7-11 PMID: 18315869

21. Golestanirad L, Angelone LM, Iacono MI, Katnani H, Wald LL, Bonmassar G. Local SAR near deep brain stimulation (DBS) electrodes at 64 and 127 MH z: A simulation study of the effect of extracranial loops. Magnetic resonance in medicine. 2017; 78(4):1558–65. https://doi.org/10.1002/mrm.26535 PMID: 27797157

22. McElcheran C, Yang B, Tam F, Golestanirad L, Graham S. Heterogeneous gelatin-based head phantom for evaluating DBS heating. Proc Intl Soc Mag Reson Med. 2016; 24:2222.

23. Bhusal B, Nguyen BT, Vu J, Elahi B, Rosenow J, Nolt MJ, et al., editors. Device Configuration and Patient's Body Composition Significantly Affect RF Heating of Deep Brain Stimulation Implants During MRI: An Experimental Study at 1.5 T and 3T. 2020 42nd Annual International Conference of the IEEE Engineering in Medicine & Biology Society (EMBC); 2020: IEEE.

24. Dielectric Properties of Body Tissues (http://niremf.ifac.cnr.it/tissprop/htmlclie/htmlclie.php). Italian National Research Council Accessed 2020.

25. Zhang M, Che Z, Chen J, Zhao H, Yang L, Zhong Z, et al. Experimental determination of thermal conductivity of water− agar gel at different concentrations and temperatures. Journal of Chemical & Engineering Data. 2011; 56(4):859–64.

26. Tissue Properties: Thermal Conductivity (https://itis.swiss/virtual-population/tissue-properties/database/thermal-conductivity). ITIS Foundation Accessed 2020.

27. Golestanirad L, Pilitsis J, Martin A, Larson P, Keil B, Bonmassar G, editors. Variation of RF heating around deep brain stimulation leads during 3.0 T MRI in fourteen patient-derived realistic lead models: The role of extracranial lead management. 25th Annual Meeting of the International Sosciety of Magnetic Resonance in Medicine; 2017.

28. Bhusal B, Rosenow J, Nolt M, Lopez-Rosado R, Pilitsis J, Golestanirad L. Surgical modification of extracranial trajectories of DBS leads can significantly reduce image artifact and RF heating during MRI at 3T. Proc Intl Soc Mag Reson Med28. 2020:1124.

29. Global Opportunity Analysis and Industry Forecast, 2014–2022: Medical Implants Market By Type (Orthopedic Implants, cardiac implants, Stents, Spinal Implants, Neurostimulators, dental implants, Breast Implants, facial Implants) and By Materials (Metallic, Ceramic, Polymers, Natural) (https://www.alliedmarketresearch.com/request-sample/71) Accessed 2020.

30. He W, Goodkind D, Kowal P. An Aging World: 2015 (https://www.census.gov/content/dam/Census/library/publications/2016/demo/p95-16-1.pdf). United States Census Bureau, 2015.

31. Kalin R, Stanton MS. Current clinical issues for MRI scanning of pacemaker and defibrillator patients. Pacing and clinical electrophysiology. 2005; 28(4):326–8. https://doi.org/10.1111/j.1540-8159.2005.50024.x PMID: 15826268

32. Naehle CP, Zeijlemaker V, Thomas D, Meyer C, Strach K, Fimmers R, et al. Evaluation of cumulative effects of MR imaging on pacemaker systems at 1.5 Tesla. Pacing and clinical electrophysiology. 2009; 32(12):1526–35. https://doi.org/10.1111/j.1540-8159.2009.02570.x PMID: 19793358

33. Rezai AR, Finelli D, Nyenhuis JA, Hrdlicka G, Tkach J, Sharan A, et al. Neurostimulation systems for deep brain stimulation: In vitro evaluation of magnetic resonance imaging–related heating at 1.5 tesla. Journal of Magnetic Resonance Imaging. 2002; 15(3):241–50. https://doi.org/10.1002/jmri.10069 PMID: 11891968

34. Baker KB, Tkach JA, Nyenhuis JA, Phillips M, Shellock FG, Gonzalez-Martinez J, et al. Evaluation of specific absorption rate as a dosimeter of MRI-related implant heating. Journal of Magnetic Resonance Imaging. 2004; 20(2):315–20. https://doi.org/10.1002/jmri.20103 PMID: 15269959

35. Bhusal B, Bhattacharyya P, Baig T, Jones S, Martens MJMrim. Measurements and simulation of RF heating of implanted stereo-electroencephalography electrodes during MR scans. Magnetic Resonance in Medicine. 2018; 80(4):1676–85. https://doi.org/10.1002/mrm.27144 PMID: 29468721

36. Henderson JM, Tkach J, Phillips M, Baker K, Shellock FG, Rezai AR. Permanent neurological deficit related to magnetic resonance imaging in a patient with implanted deep brain stimulation electrodes for Parkinson's disease: case report. Neurosurgery. 2005; 57(5):E1063. https://doi.org/10.1227/01.neu.0000180810.16964.3e PMID: 16284543

37. Kerl HU, Gerigk L, Pechlivanis I, Al-Zghloul M, Groden C, Nölte IJJon. The subthalamic nucleus at 3.0 Tesla: choice of optimal sequence and orientation for deep brain stimulation using a standard installation protocol. 2012; 117(6):1155–65.

38. Cheng C-H, Huang H-M, Lin H-L, Chiou S-M. 1.5 T versus 3T MRI for targeting subthalamic nucleus for deep brain stimulation. British journal of neurosurgery. 2014; 28(4):467–70. https://doi.org/10.3109/02688697.2013.854312 PMID: 24191703

39. Alkemade A, de Hollander G, Keuken MC, Schäfer A, Ott DV, Schwarz J, et al. Comparison of T2*-weighted and QSM contrasts in Parkinson's disease to visualize the STN with MRI. PloS one. 2017; 12(4):e0176130. https://doi.org/10.1371/journal.pone.0176130 PMID: 28423027

40. Liu T, Eskreis-Winkler S, Schweitzer AD, Chen W, Kaplitt MG, Tsiouris AJ, et al. Improved subthalamic nucleus depiction with quantitative susceptibility mapping. Radiology. 2013; 269(1):216–23. https://doi.org/10.1148/radiol.13121991 PMID: 23674786

41. Schneider TM, Deistung A, Biedermann U, Matthies C, Ernestus R-I, Volkmann J, et al. Susceptibility sensitive magnetic resonance imaging displays pallidofugal and striatonigral fiber tracts. 2016; 12(4):330–8.

42. McElcheran CE, Yang B, Anderson KJ, Golestanirad L, Graham S. Parallel radiofrequency transmission at 3 tesla to improve safety in bilateral implanted wires in a heterogeneous model. Magnetic resonance in medicine. 2017; 78(6):2406–15. https://doi.org/10.1002/mrm.26622 PMID: 28244142

43. McElcheran C, Golestanirad L, Iacono M, Wei P-S, Yang B, Anderson K, et al. Numerical simulations of realistic lead trajectories and an experimental verification support the efficacy of parallel radiofrequency transmission to reduce heating of deep brain stimulation implants during MRI. Scientific reports. 2019; 9(1):1–14. https://doi.org/10.1038/s41598-018-37186-2 PMID: 30626917

44. Kazemivalipour E, Keil B, Vali A, Rajan S, Elahi B, Atalar E, et al. Reconfigurable MRI technology for low-SAR imaging of deep brain stimulation at 3T: Application in bilateral leads, fully-implanted systems, and surgically modified lead trajectories. NeuroImage. 2019; 199:18–29. https://doi.org/10.1016/j.neuroimage.2019.05.015 PMID: 31096058

45. Guerin B, Angelone LM, Dougherty D, Wald LL. Parallel transmission to reduce absorbed power around deep brain stimulation devices in MRI: Impact of number and arrangement of transmit channels. Magnetic resonance in medicine. 2020; 83(1):299–311. https://doi.org/10.1002/mrm.27905 PMID: 31389069

46. Golestanirad L, Kazemivalipour E, Keil B, Downs S, Kirsch J, Elahi B, et al. Reconfigurable MRI coil technology can substantially reduce RF heating of deep brain stimulation implants: First in-vitro study of RF heating reduction in bilateral DBS leads at 1.5 T. PloS one. 2019; 14(8):e0220043. https://doi.org/10.1371/journal.pone.0220043 PMID: 31390346

47. Etezadi-Amoli M, Stang P, Kerr A, Pauly J, Scott G. Controlling radiofrequency-induced currents in guidewires using parallel transmit. Magnetic resonance in medicine. 2015; 74(6):1790–802. https://doi.org/10.1002/mrm.25543 PMID: 25521751

48. McElcheran C, Golestanirad L, Iacono M, Yang B, Anderson K, Bonmassar G, et al., editors. Parallel transmission for heating reduction in realistic deep brain stimulation lead trajectories. Proc Intl Soc Mag Reson Med; 2017.

49. McElcheran CE, Yang B, Anderson KJ, Golenstani-Rad L, Graham SJ. Investigation of parallel radiofrequency transmission for the reduction of heating in long conductive leads in 3 Tesla magnetic resonance imaging. PLoS One. 2015; 10(8):e0134379. https://doi.org/10.1371/journal.pone.0134379 PMID: 26237218

50. Golestanirad L, Kirsch J, Bonmassar G, Downs S, Elahi B, Martin A, et al. RF-induced heating in tissue near bilateral DBS implants during MRI at 1.5 T and 3T: The role of surgical lead management. NeuroImage. 2019; 184:566–76. https://doi.org/10.1016/j.neuroimage.2018.09.034 PMID: 30243973

51. Olsen JM, Hrdlicka GA, Wahlstrand CD, Hoegh TB, inventorsLead electrode for use in an MRI-safe implantable medical device. US Patent US7877150B22010.

52. McCabe S, Scott J. A Novel Implant Electrode Design Safe in the RF Field of MRI Scanners. IEEE Transactions on Microwave Theory and Techniques. 2017. https://doi.org/10.1109/TMTT.2016.2638423 PMID: 28507391

53. Stevenson RA, Halperin HR, Lardo AC, Dabney WS, Kondabatni KK, Frysz CA, et al., inventorsImplantable lead bandstop filter employing an inductive coil with parasitic capacitance to enhance MRI compatibility of active medical devices. U sPatent US8903505B22012.

54. Vase A, Sethna DN, inventorsImplantable medical lead configured for improved mri safety. US Patent US20090270956A12008.

55. Atalar E, Allen J, Bottomley P, Eldelstein W, Karmarkar PV, inventorsMRI-safe high impedance lead systems. US Patent US8055351B22011.

56. Golestanirad L, Angelone LM, Kirsch J, Downs S, Keil B, Bonmassar G, et al. Reducing RF-induced heating near implanted leads through high-dielectric capacitive bleeding of current (CBLOC). IEEE transactions on microwave theory and techniques. 2019; 67(3):1265–73. https://doi.org/10.1109/TMTT.2018.2885517 PMID: 31607756

57. Serano P, Angelone LM, Katnani H, Eskandar E, Bonmassar G. A novel brain stimulation technology provides compatibility with MRI. Scientific reports. 2015;5. https://doi.org/10.1038/srep09805 PMID: 25924189

58. Boutet A, Rashid T, Hancu I, Elias GJ, Gramer RM, Germann J, et al. Functional MRI safety and artifacts during deep brain stimulation: experience in 102 patients. Radiology. 2019; 293(1):174–83. https://doi.org/10.1148/radiol.2019190546 PMID: 31385756

59. Hancu I, Boutet A, Fiveland E, Ranjan M, Prusik J, Dimarzio M, et al. On the (Non-) equivalency of monopolar and bipolar settings for deep brain stimulation fMRI studies of Parkinson's disease patients. Journal of Magnetic Resonance Imaging. 2019; 49(6):1736–49. https://doi.org/10.1002/jmri.26321 PMID: 30552842

60. Golestanirad L, Rahsepar AA, Kirsch JE, Suwa K, Collins JC, Angelone LM, et al. Changes in the specific absorption rate (SAR) of radiofrequency energy in patients with retained cardiac leads during MRI at 1.5 T and 3T. Magnetic resonance in medicine. 2019; 81(1):653–69. https://doi.org/10.1002/mrm.27350 PMID: 29893997

61. Golestanirad L, Kazemivalipour E, Lampman D, Habara H, Atalar E, Rosenow J, et al. RF heating of deep brain stimulation implants in open-bore vertical MRI systems: A simulation study with realistic device configurations. Magnetic resonance in medicine. 2020; 83(6):2284–92. https://doi.org/10.1002/mrm.28049 PMID: 31677308

62. Kazemivalipour E, Vu J, Lin S, Bhusal B, Nguyen BT, Kirsch J, et al., editors. RF heating of deep brain stimulation implants during MRI in 1.2 T vertical scanners versus 1.5 T horizontal systems: A simulation study with realistic lead configurations. 2020 42nd Annual International Conference of the IEEE Engineering in Medicine & Biology Society (EMBC); 2020: IEEE.

63. Wei P, Yang B, McElcheran C, Golestanirad L, Graham S, editors. Reducing radiofrequency-induced heating in realistic deep brain stimulation lead trajectories using parallel transmission. Proc Int Soc Magn Reson Med; 2018.

64. Mavridis I, Boviatsis E, Anagnostopoulou SJAri. Anatomy of the human subthalamic nucleus: a combined morphometric study. 2013.

65. Hargreaves BA, Worters PW, Pauly KB, Pauly JM, Koch KM, Gold GEJAJoR. Metal-induced artifacts in MRI. 2011; 197(3):547–55.